



Observation of exotic $J/\psi\phi$ resonances in diffractive processes in proton-proton collisions

LHCb collaboration[†]

Abstract

The first study of $J/\psi\phi$ production in diffractive processes in proton-proton collisions is presented. The study is based on an LHCb dataset recorded at centre-of-mass energy of 13 TeV, corresponding to an integrated luminosity of 5 fb^{-1} . The data disfavour a nonresonant $J/\psi\phi$ production but are consistent with a resonant model including several resonant states observed previously only in $B^+ \rightarrow J/\psi\phi K^+$ decays. The $\chi_{c0}(4500)$ state is observed with a significance over 5σ and the $\chi_{c1}(4274)$ is confirmed with a significance of more than 4σ .

Submitted to Phys. Rev. Lett.

© 2024 CERN for the benefit of the LHCb collaboration. CC BY 4.0 licence.

[†]Authors are listed at the end of this paper.

Studies of exclusive hadronic processes in proton-proton (pp) collisions have been proposed to clarify poorly understood phenomena associated with the asymptotic high-energy behaviour of quantum chromodynamics (QCD) [1]. In particular, it remains theoretically challenging to describe the production of complex states, such as vector-meson pairs, in central diffractive collisions with large rapidity gaps. Photon-induced or pomeron-induced processes have been proposed to understand the QCD dynamics at high energies [2] including the production of exotic states and double vector-meson production [3–9]. The discovery of exotic QCD states has motivated an extensive theoretical and experimental effort to understand their properties [10]. The nature of exotic hadrons has been studied mainly in inclusive production or in exclusive beauty hadron decays, in terms of properties such as mass, spin and decay width. Resonant structures in the $J/\psi\phi$ mass spectrum have previously been observed in amplitude analyses of $B^+ \rightarrow J/\psi\phi K^+$ decays [11–13]. Five of those exotic candidates, $\chi_{c1}(4140)$, $\chi_{c1}(4274)$ and $\chi_{c1}(4685)$ with quantum numbers $J^{PC} = 1^{++}$ and $\chi_{c0}(4500)$ and $\chi_{c0}(4700)$ with $J^{PC} = 0^{++}$, can be produced in photon-photon or pomeron-pomeron processes, with the latter expected to dominate in pp collisions. Searches for the production of these exotic-hadron candidates in such processes can help elucidate their nature and distinguish between compact tetraquarks and molecular states [14–17].

In this Letter, the $J/\psi(\rightarrow \mu^+\mu^-)\phi(\rightarrow K^+K^-)$ production cross-section is measured for the first time in events with no additional detected activity, in which photon- and pomeron-induced processes are expected to be dominant. An analysis of the $J/\psi\phi$ invariant-mass distribution is also performed and production cross-sections are determined for each of the five resonant states and a nonresonant (NR) component. The data used correspond to an integrated luminosity of 5 fb^{-1} collected in pp collisions at $\sqrt{s} = 13 \text{ TeV}$ with the LHCb detector.

The LHCb detector is a single-arm forward spectrometer covering the pseudorapidity range $2 < \eta < 5$, described in detail in Refs. [18,19]. The HERSCHEL detector [20] extends the LHCb coverage to the pseudorapidity range $5 < |\eta| < 10$, increasing sensitivity to proton dissociation background. A simulated dataset of $pp \rightarrow p + J/\psi\phi + p$ events is created using the SUPERCHIC3 package [3,21], by generating $pJ/\psi J/\psi p$ events and replacing one of the J/ψ states with a ϕ resonance. Final-state radiation is simulated using the PHOTOS package [22]. The interaction of the generated particles with the detector material, and the detector response, are simulated using the GEANT4 toolkit [23,24] as described in Ref. [25]. Samples of photoproduced J/ψ mesons, generated with SUPERCHIC2 [26], are used to constrain the J/ψ mass model.

The $X \rightarrow J/\psi\phi$ candidate decays, where X indicates a hypothetical resonance, are selected online by a two-stage trigger optimised to identify low-multiplicity events with at least one muon. The first stage requires fewer than 20 deposits in the scintillating-pad detector (SPD) of the calorimeter system and at least one muon candidate with a transverse momentum (p_T) greater than 200 MeV.¹ The second stage applies a full event reconstruction and requires fewer than eight tracks with pseudorapidity $2 < \eta < 5$ (forward tracks), no tracks with pseudorapidity $-3.5 < \eta < -1.5$ (backward tracks) and at least one track identified as a muon with p_T above 400 MeV.

Additional geometric and kinematic requirements are applied to events selected by the trigger system. Particle identification information is used to select two kaon and

¹Natural units with $\hbar = c = 1$ are used throughout.

two muon candidates, which must also have p_T above 200 MeV and be in the region $2 < \eta < 5$. At least one muon candidate is required to be responsible for the event passing the hardware and software stages of the trigger. Events with additional activity, *i.e.*, with additional tracks reconstructed in the vertex detector (VELO tracks), are vetoed. The dimuon (dikaon) invariant mass is required to be in the range $3036 < M_{\mu\mu} < 3156$ MeV ($1005 < M_{KK} < 1035$ MeV). The $J/\psi\phi$ invariant mass is required to be less than 6000 MeV. After the selection requirements, 989 $J/\psi\phi$ candidates are retained.

No requirements are applied to discriminate events in which the outgoing protons stay intact from those where one or both of the protons dissociate. Instead, a variable that quantifies activity above noise in the HERSCHEL detector is used to estimate the fraction for each of these cases. The efficiency of such a classification is determined using the same method described in Ref. [27] and it is found that at least 69% of the $J/\psi\phi$ candidates are produced in events in which one or both protons dissociate.

The requirement of no additional activity results in the rejection of events that are accompanied by additional visible pp interactions in the same bunch crossing. Correspondingly, a single-interaction integrated luminosity (\mathcal{L}_{eff}) must be determined to evaluate the cross-section. The number of visible pp interactions per bunch crossing is assumed to follow a Poisson distribution. The mean is determined using the fraction of beam crossings with no visible activity, *i.e.*, with no reconstructed VELO tracks. The effective single-interaction integrated luminosity is found to be about 1.75 fb^{-1} . The integrated cross-section is then calculated as

$$\sigma = \frac{\mathcal{P} \cdot N}{\varepsilon \cdot \mathcal{L}_{\text{eff}}}, \quad (1)$$

where N is the total event yield (or individual component yield), \mathcal{P} is the sample purity and ε is the total efficiency, which includes reconstruction and selection efficiencies. Note that 46 of the selected events were collected during moments in which the luminosity could not be reliably measured. Therefore, these events are excluded from the cross-section calculation.

In order to estimate the sample purity, *i.e.* the fraction of events with resonant dimuon and dikaon production, a two-dimensional unbinned extended maximum-likelihood fit is performed on the dimuon and dikaon invariant-mass distributions. For this, the invariant-mass window requirements are relaxed to $1500 < M_{\mu\mu} < 4500$ MeV and $990 < M_{KK} < 1190$ MeV. The J/ψ contribution is modelled by a double-sided Crystal Ball function [28] with tail parameters determined from simulation, while the $\psi(2S)$ is modelled by a Gaussian function and the nonresonant $\mu^+\mu^-$ background with an exponential function. The ϕ contribution is modelled by a relativistic Breit–Wigner function convolved with a Gaussian function, while the nonresonant K^+K^- background is described by a uniform distribution. The sample purity is found to be $(93.0 \pm 0.5)\%$. The dimuon and dikaon invariant-mass distributions, together with the projections of the fit result, can be found in the supplemental material. The efficiency of the mass-window requirement is estimated as the fraction of events in the mass window with respect to the relaxed mass range. The dimuon and dikaon invariant-mass distributions, along with the projections of the fit result, are shown in Fig. 1.

The efficiency of the SPD requirement is estimated using a combination of simulation and data samples. The simulated SPD multiplicity from signal events is convolved with the distribution of spillover SPD hits from the previous bunch crossing in data, obtained

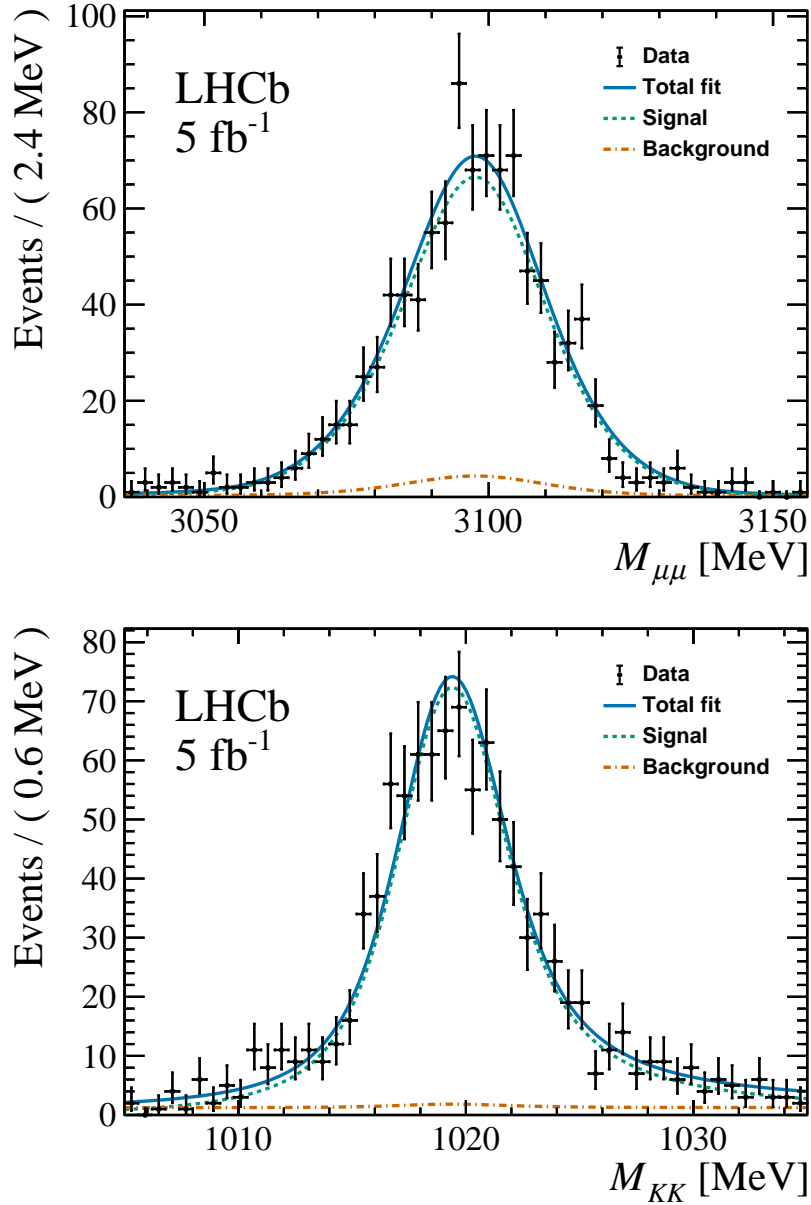


Figure 1: (Top) Dimuon and (bottom) dikaon invariant-mass distributions within the invariant-mass selection windows. The projections of the two-dimensional unbinned fit are overlaid. The signal component consists of $J/\psi\phi$ candidates. The peaking behaviour of the background arises when one of the pairs ($\mu\mu$ or KK) is background.

from events with no visible activity, and the fraction of events passing the requirement is determined. The efficiency of vetoing additional VELO tracks is studied using simulation.

The reconstruction efficiencies are obtained from simulation, and correspond to the fraction of charged particles produced in the LHCb angular acceptance that are reconstructed as tracks. The simulated sample is also used to determine the muon-system acceptance, which is calculated as the fraction of reconstructed muons that cross the LHCb muon system. The muon identification efficiency is obtained with a data-driven method using a sample of $J/\psi \rightarrow \mu^+\mu^-$ decays in low multiplicity events. The same data sample is used to calculate the muon trigger efficiency. Since the muon trigger requirements include

muon identification, this efficiency is calculated for identified muons that satisfy the muon trigger requirements. The efficiency for kaon identification is obtained with a data-driven method using a sample of $\phi \rightarrow K^+K^-$ decays in low multiplicity events. The muon and kaon detection efficiencies, which are computed as functions of p_T and η , are assumed to factorise. The overall selection efficiency is found to be $(19.90 \pm 0.32)\%$, where the uncertainty is statistical.

The $J/\psi\phi$ invariant-mass spectrum is described by a model consisting of five resonances, namely $\chi_{c1}(4140)$, $\chi_{c1}(4274)$, $\chi_{c0}(4500)$, $\chi_{c1}(4685)$ and $\chi_{c0}(4700)$, and a nonresonant component. The resonances considered are the ones observed in Refs. [11–13] with quantum numbers compatible with exclusive photon-induced or pomeron-induced production processes. The resonant components are described by relativistic Breit–Wigner distributions convolved with Gaussian functions to account for detector resolution effects. The resolutions are estimated from simulation. Due to the small sample size, the mass and width of the less significant resonances ($\chi_{c1}(4140)$, $\chi_{c1}(4685)$ and $\chi_{c0}(4700)$) are fixed to the values observed in Ref. [13] and it is assumed that there is no interference between the fit components. Moreover, only the combined $\chi_{c1}(4685) + \chi_{c0}(4700)$ yield is estimated since it is not possible to resolve the $\chi_{c1}(4685)$ and $\chi_{c0}(4700)$ states. The nonresonant component is modelled by an exponential distribution modified with a parametrised factor to account for the $J/\psi\phi$ mass threshold,

$$f_{\text{NR}} = \left[1 - \exp\left(a \cdot \left(\frac{M_{J/\psi\phi}}{m_T} - 1\right)\right) \right] \cdot \exp\left(b \cdot \frac{M_{J/\psi\phi}}{m_T}\right), \quad (2)$$

where m_T is the $J/\psi\phi$ mass threshold, a is the coefficient representing the strength of the threshold effect and b is the slope of the exponential distribution. The nonresonant component is also convolved with a Gaussian function to account for detector resolution.

The parameter a is determined separately using a sideband sample, which is obtained by applying all selection requirements, except for an inverted offline multiplicity requirement of more than four VELO tracks. Figure 2 shows the result of a maximum-likelihood fit performed on the resulting distribution using a model that consists of a sum of two exponential functions modified by the turn-on factor described in Eq. 2 and convolved with the same resolution function. This distribution shows no clear mass structure, however when imposing the exclusivity requirement a resonant structure appears, which indicates the presence of a photon-induced or pomeron-induced mechanism. The resulting $J/\psi\phi$ invariant-mass distribution for signal candidates is shown in Fig. 3 overlaid with the results of an extended maximum-likelihood fit of the signal model.

The sources of systematic uncertainties considered for the cross-section measurement are summarised below. The integrated luminosity is determined with a precision of 2% [29]. The uncertainty on the SPD requirement efficiency, which accounts for possible mismodeling of the SPD distribution, is estimated to be 1.3% by shifting the model until it no longer describes data. The systematic uncertainty due to the size of the simulated sample used to estimate the efficiency for vetoing additional VELO tracks is found to be smaller than 0.1%. The muon trigger, muon identification and kaon identification efficiencies uncertainties due to the limited data samples are found to be below 0.2%.

Systematic uncertainties related to the sample purity and efficiency of invariant-mass requirements were determined from the two-dimensional fit and are 0.5% and 0.04%, respectively. Furthermore, an alternative parametrisation of the background in the dikaon invariant-mass spectrum is evaluated, which consists of a second-order polynomial.

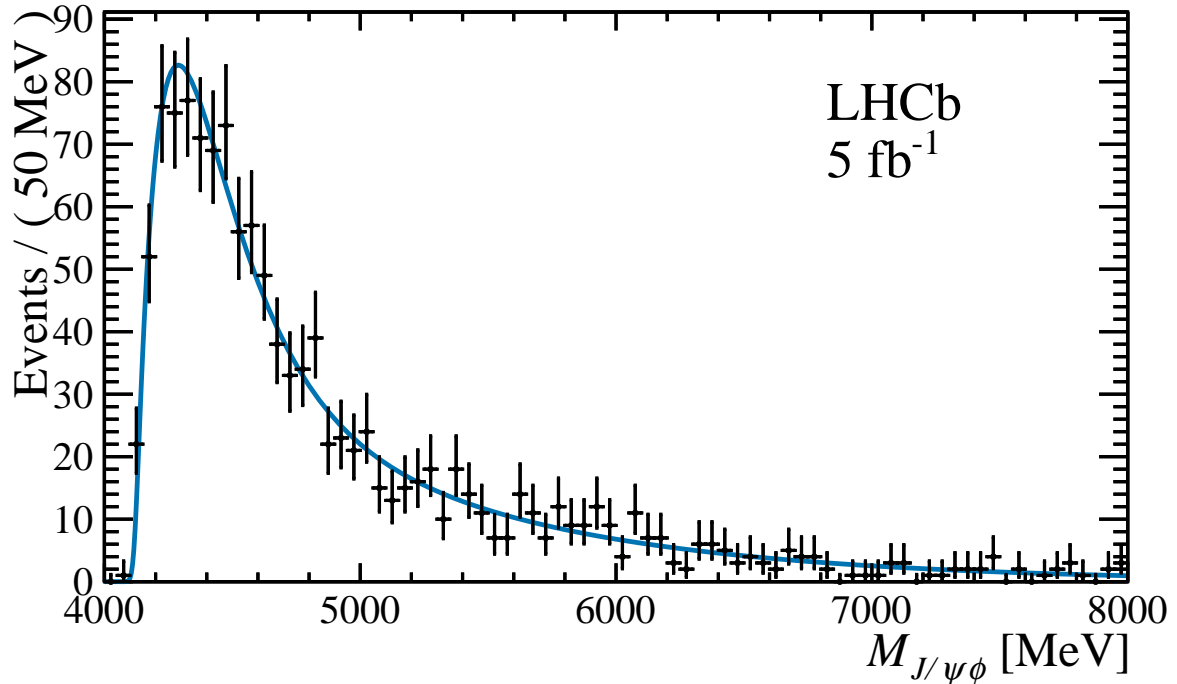


Figure 2: Invariant-mass distribution of $J/\psi\phi$ candidates for the sideband sample composed of events with more than four reconstructed VELO tracks. Note that all other selection requirements are applied, including the J/ψ and ϕ mass-window requirements. The fit results are shown as a solid line.

This causes a 0.4% variation in the sample purity, which is added to the corresponding systematic uncertainty, resulting in a overall uncertainty of 0.7%. An additional systematic uncertainty is considered for the cross-section of the individual $J/\psi\phi$ components due to the possible dependence of the purity on the $J/\psi\phi$ invariant mass. The two-dimensional fit to the dimuon and dikaon invariant-mass distributions shows that the background is dominated by $J/\psi K^+ K^-$ candidates. A fit to the $J/\psi K^+ K^-$ invariant-mass distribution is performed using events selected with $1050 < M_{KK} < 1200$ MeV. The change in the relative contribution of the resonant and nonresonant components is found to be 0.5% and 2.4%, respectively, and is taken as systematic uncertainty.

The systematic uncertainties on the kaon and muon reconstruction efficiencies and muon system acceptance due to the limited simulation sample size are found to be negligible. To account for the systematic uncertainty due to the discrepancies between data and simulation in the tracking efficiency, a 0.4% systematic uncertainty per track and an additional 1.4% systematic uncertainty per hadron is included [30], which amounts to an extra 3.2% systematic uncertainty.

The factorisation hypothesis employed for the efficiencies is tested using simulation. Simulated $J/\psi(\rightarrow \mu^+ \mu^-)\phi(\rightarrow K^+ K^-)$ events are selected by requiring that the kaon and muon tracks satisfy the nominal p_T and η selection requirements, that the kaons and muons are reconstructed, and that the muons are within the muon system acceptance. The resulting $M_{J/\psi\phi}$ distribution is then corrected by the reconstruction efficiencies and muon system acceptance. The corrected distribution is compared to the mass distribution without the reconstruction requirements after weighting the simulated events to have the

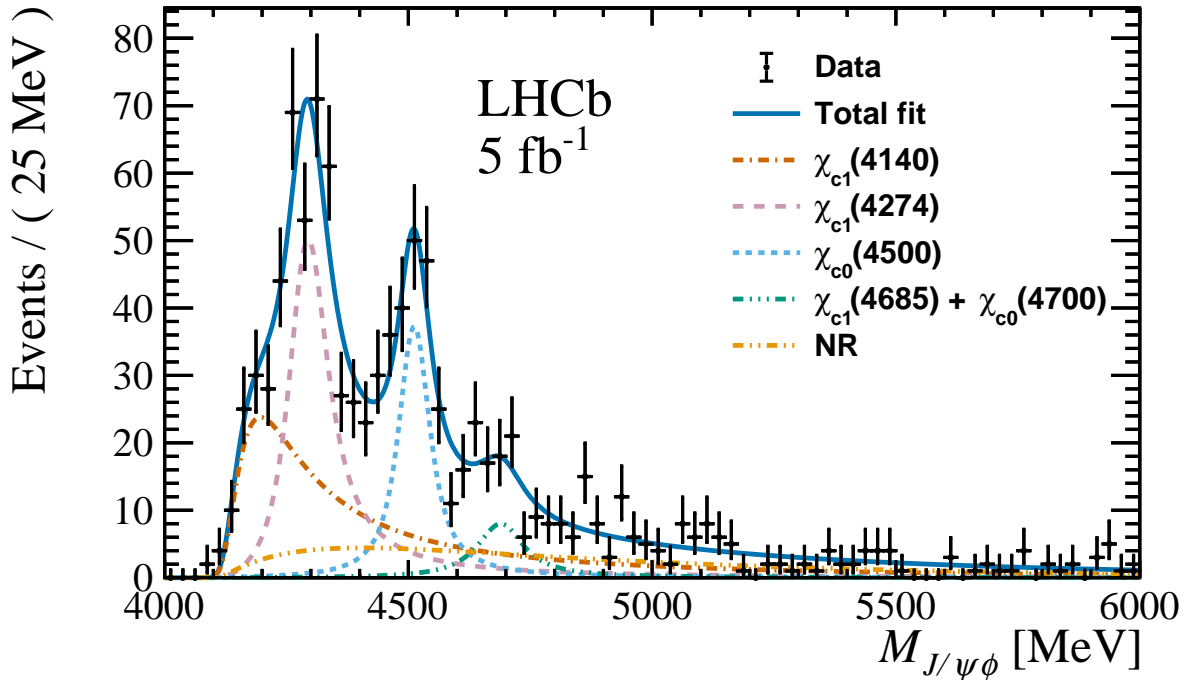


Figure 3: Invariant-mass distribution of $J/\psi(\rightarrow \mu^+\mu^-)\phi(\rightarrow K^+K^-)$ candidates in the signal sample after selection. The fit components are shown as dashed lines.

same two-dimensional rapidity distribution, $y_{J/\psi} \times y_\phi$, as obtained in data. It is found that the shapes of the distribution with no reconstruction requirements and the one corrected by the efficiencies are consistent. However, the normalisation is underestimated by about 3%, which is included as a systematic uncertainty. The total relative systematic uncertainty of the total cross-section is 5.6%.

To assess the systematic uncertainty on the $J/\psi\phi$ invariant-mass fit parameters, a weighted fit is performed with each event-dependent correction varied within its uncertainty. The threshold-effect strength parameter is varied within its uncertainties to study the impact of its precision. Systematic uncertainties due to the $J/\psi\phi$ mass resolution determination are also considered, taking into account the precision of the Gaussian resolution and the choice of the resolution model.

To estimate the systematic uncertainties due to the fixed parameters in the model, the $J/\psi\phi$ invariant-mass fit is repeated with one mean and width pair allowed to vary at a time within the uncertainties quoted in Ref. [13]. The resulting discrepancy on the remaining parameters with respect to the baseline fit is taken as a systematic uncertainty. Systematic uncertainties due to unknown interference effects between the fit components are also considered. These are estimated by repeating the $J/\psi\phi$ invariant-mass fits and allowing for interference between certain states with the same quantum numbers. Interference is only considered between the $\chi_{c1}(4140)$ and $\chi_{c1}(4274)$ (1^{++}) states, the $\chi_{c0}(4500)$ and $\chi_{c0}(4700)$ (0^{++}) states, and the $\chi_{c0}(4500)$ state and the nonresonant component (0^{++}).

The dominant sources of systematic uncertainties are summarised in Table 1 for the measured cross-sections, means and widths. Moreover, the masses and widths obtained from the fit are compared to those in Ref. [13] in Table 2. The observed parameters are found to be in agreement with the previous LHCb measurement, except for the $\chi_{c0}(4500)$

mass, which is observed to have a higher value in this analysis.

Table 1: Summary of systematic uncertainties in the production cross-section (σ), mass (M) and width (Γ) of the measured resonant states. The contributions that affect the total uncertainty by less than 5% are omitted. The two leftmost sources represent the contributions due to fixed parameters. The contribution due to the precision of the $J/\psi\phi$ invariant-mass resolution determination is indicated as ΔM . The contributions due to unknown interference effects between $\chi_{c1}(4140)$ and $\chi_{c1}(4274)$, $\chi_{c0}(4500)$ and $\chi_{c0}(4700)$, and $\chi_{c0}(4500)$ and the nonresonant component are indicated as δ_1 , δ_2 and δ_3 , respectively.

Source	$\chi_{c1}(4140)$	$\chi_{c0}(4700)$	ΔM	δ_1	δ_2	δ_3	Total
$M_{\chi_{c1}(4274)}$ [MeV]	1.7	0.2	1.5	8.0	0.2	2.9	8.9
$\Gamma_{\chi_{c1}(4274)}$ [MeV]	10	0.3	0.7	56	0.8	6.2	57
$M_{\chi_{c0}(4500)}$ [MeV]	0.4	0.4	1.4	0.6	1.6	2.0	3.0
$\Gamma_{\chi_{c0}(4500)}$ [MeV]	1.7	0.2	2.0	3.4	4.4	31	32
$\sigma_{\chi_{c1}(4140)}$	31%	1.5%	0.9%	11%	1.5%	8.3%	35%
$\sigma_{\chi_{c1}(4274)}$	19%	1.6%	0.8%	11%	1.6%	5.8%	24%
$\sigma_{\chi_{c0}(4500)}$	3.2%	0.7%	0.2%	6.5%	11%	5.1%	15%
$\sigma_{\chi_{c1}(4685)}$ + $\chi_{c0}(4700)$	5.3%	18%	7.3%	3.1%	13%	31%	41%

Table 2: Mass and width parameters obtained from the fit to the $J/\psi\phi$ invariant-mass distribution. The first uncertainty is statistical, while the second is systematic. The results of this analysis are compared to the ones observed in Ref. [13].

Parameter [MeV]	Current analysis	Ref. [13]
$M_{\chi_{c1}(4274)}$	$4298 \pm 6 \pm 9$	$4294 \pm 4_{-6}^{+3}$
$\Gamma_{\chi_{c1}(4274)}$	$92_{-18}^{+22} \pm 57$	$53 \pm 5 \pm 5$
$M_{\chi_{c0}(4500)}$	$4512.5_{-6.2}^{+6.0} \pm 3.0$	$4474 \pm 3 \pm 3$
$\Gamma_{\chi_{c0}(4500)}$	$65_{-16}^{+20} \pm 32$	$77 \pm 6_{-8}^{+10}$

In the fiducial region defined by $M_{J/\psi\phi} < 6000$ MeV and muon and kaon candidates with $2 < \eta < 5$ and $p_T > 200$ MeV, and one muon candidate with $p_T > 400$ MeV, the resulting $J/\psi(\rightarrow \mu^+\mu^-)\phi(\rightarrow K^+K^-)$ production cross-section with no additional activity in the event is found to be

$$\begin{aligned} \sigma_{J/\psi\phi} \times \mathcal{B}(J/\psi \rightarrow \mu^+\mu^-) \times \mathcal{B}(\phi \rightarrow K^+K^-) \\ = (2.52 \pm 0.08 \pm 0.12 \pm 0.05) \text{ pb}, \end{aligned}$$

where the first uncertainty is statistical, the second is systematic and the third is due to the luminosity determination. The individual production cross-sections for each of the

observed resonant states are found to be

$$\begin{aligned}
\sigma_{\chi_{c1}(4140)} \times \mathcal{B}_{\text{eff}}^{\chi_{c1}(4140)} &= (0.80 \pm 0.15 \pm 0.28) \text{ pb}, \\
\sigma_{\chi_{c1}(4274)} \times \mathcal{B}_{\text{eff}}^{\chi_{c1}(4274)} &= (0.73 \pm 0.08 \pm 0.17) \text{ pb}, \\
\sigma_{\chi_{c0}(4500)} \times \mathcal{B}_{\text{eff}}^{\chi_{c0}(4500)} &= (0.42_{-0.08}^{+0.09} \pm 0.06) \text{ pb}, \\
\sigma_{\chi_{c1}(4685)+\chi_{c0}(4700)} & \\
\times \mathcal{B}_{\text{eff}}^{\chi_{c1}(4685)+\chi_{c0}(4700)} &= (0.14_{-0.06}^{+0.07} \pm 0.06) \text{ pb}, \\
\sigma_{\text{NR}} \times \mathcal{B}_{\text{eff}}^{\text{NR}} &= (0.43_{-0.18}^{+0.24} \pm 0.20) \text{ pb},
\end{aligned}$$

where the first uncertainty is statistical, while the second is the systematic uncertainty combined with the luminosity determination uncertainty. Here, $\mathcal{B}_{\text{eff}}^X = \mathcal{B}(X \rightarrow J/\psi\phi) \times \mathcal{B}(J/\psi \rightarrow \mu^+\mu^-) \times \mathcal{B}(\phi \rightarrow K^+K^-)$, with X denoting the five resonant states in the model, and $\mathcal{B}_{\text{eff}}^{\text{NR}} = \mathcal{B}(J/\psi \rightarrow \mu^+\mu^-) \times \mathcal{B}(\phi \rightarrow K^+K^-)$.

The statistical significance for the $\chi_{c1}(4140)$ resonance is estimated via Wilks' theorem [31] since its mass and width are fixed in the fit. Even though Wilks' theorem applies strictly to cases where the resonance parameters are kept fixed, the analysis presented in this Letter follows the previous results obtained from $B^+ \rightarrow J/\psi\phi K^+$ decays [13]. Since the shape parameters of the $\chi_{c1}(4274)$ and $\chi_{c0}(4500)$ resonances approximately agree with the expectations, the estimation of the look-elsewhere effects is neglected and Wilks' theorem is applied in this case as well. Furthermore, when computing the significance of one of them, the mass and width of the others are kept fixed. The precision of the current analysis does not allow the $\chi_{c1}(4685)$ and $\chi_{c0}(4700)$ resonances to be resolved, therefore a joint significance is calculated. For the individual significances, systematic uncertainties are taken into account using the procedure employed in Ref [32]. The significance for the resonances $\chi_{c1}(4140)$, $\chi_{c1}(4274)$ and $\chi_{c0}(4500)$ are found to be 2.4σ , 4.3σ and 5.5σ . The joint $\chi_{c1}(4685) + \chi_{c0}(4700)$ significance is found to be 1.6σ .

In summary, 989 $J/\psi(\rightarrow \mu^+\mu^-)\phi(\rightarrow K^+K^-)$ candidates are observed in events without additional activity and the total fiducial cross-section is measured. Several clear resonant structures are observed in the invariant-mass distribution of these $J/\psi\phi$ candidates, which is well-described by a model containing five resonant and one nonresonant components. This is the first observation of $X \rightarrow J/\psi\phi$ production in diffractive processes and therefore helps determine the underlying nature of exotic states.

Acknowledgements

We express our gratitude to our colleagues in the CERN accelerator departments for the excellent performance of the LHC. We thank the technical and administrative staff at the LHCb institutes. We acknowledge support from CERN and from the national agencies: CAPES, CNPq, FAPERJ and FINEP (Brazil); MOST and NSFC (China); CNRS/IN2P3 (France); BMBF, DFG and MPG (Germany); INFN (Italy); NWO (Netherlands); MNiSW and NCN (Poland); MCID/IFA (Romania); MICIU and AEI (Spain); SNSF and SER (Switzerland); NASU (Ukraine); STFC (United Kingdom); DOE NP and NSF (USA). We acknowledge the computing resources that are provided by CERN, IN2P3 (France), KIT and DESY (Germany), INFN (Italy), SURF (Netherlands), PIC (Spain), GridPP (United Kingdom), CSCS (Switzerland), IFIN-HH (Romania), CBPF (Brazil), and Polish WLCG

(Poland). We are indebted to the communities behind the multiple open-source software packages on which we depend. Individual groups or members have received support from ARC and ARDC (Australia); Key Research Program of Frontier Sciences of CAS, CAS PIFI, CAS CCEPP, Fundamental Research Funds for the Central Universities, and Sci. & Tech. Program of Guangzhou (China); Minciencias (Colombia); EPLANET, Marie Skłodowska-Curie Actions, ERC and NextGenerationEU (European Union); A*MIDEX, ANR, IPhU and Labex P2IO, and Région Auvergne-Rhône-Alpes (France); AvH Foundation (Germany); ICSC (Italy); Severo Ochoa and María de Maeztu Units of Excellence, GVA, XuntaGal, GENCAT, InTalent-Inditex and Prog. Atracción Talento CM (Spain); SRC (Sweden); the Leverhulme Trust, the Royal Society and UKRI (United Kingdom).

Supplemental material

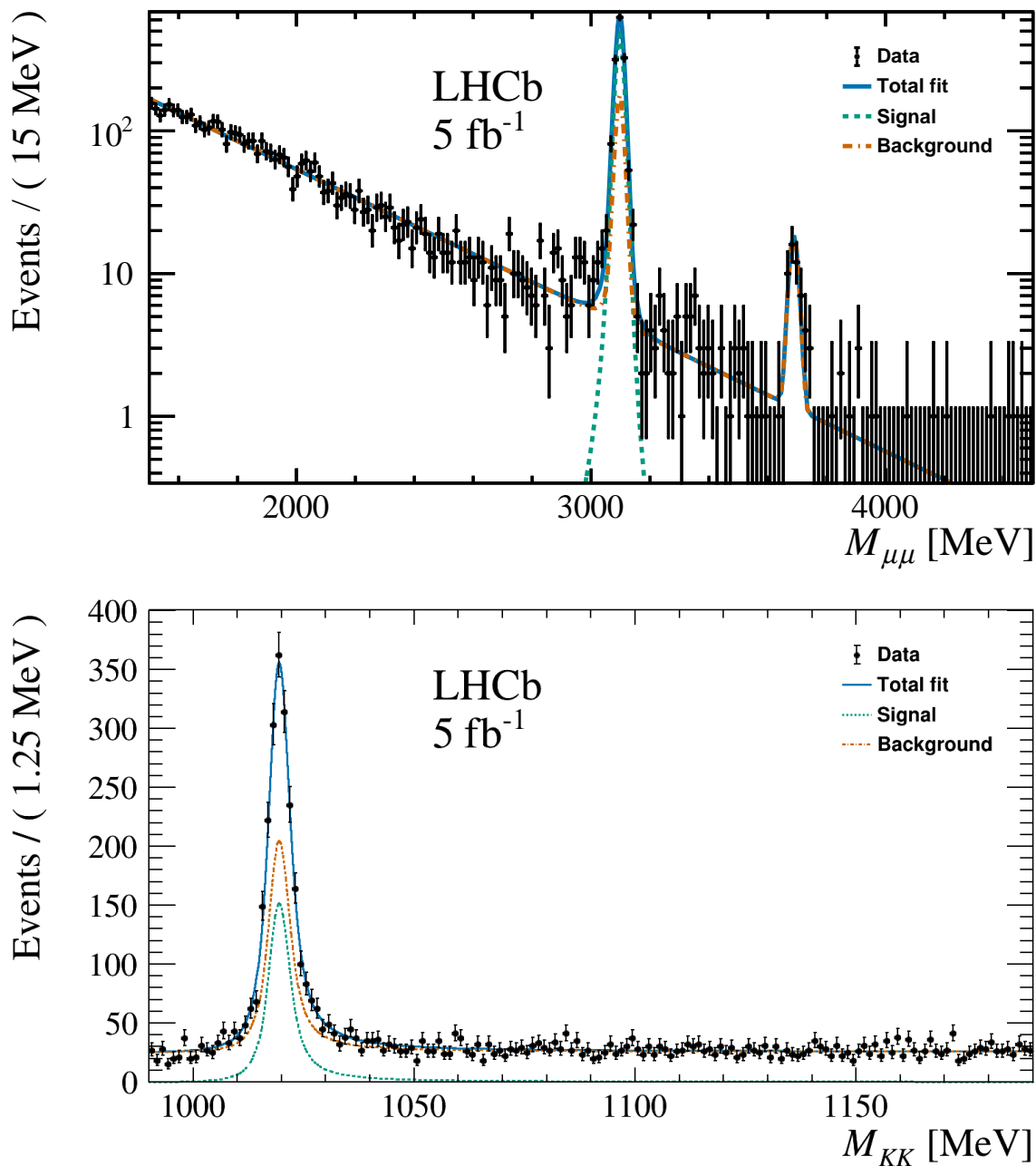











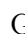




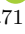
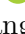



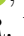




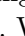


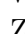





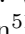


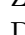
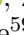



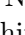
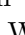


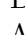
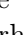
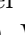



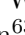


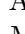
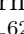


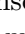
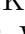

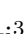

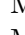

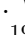

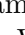


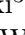

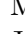

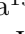



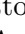



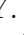
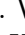

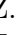

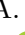
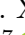

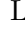
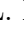


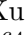








Figure 4: Dimuon (top) and dikaon (bottom) invariant-mass distributions. The projections of the two-dimensional unbinned fit are overlaid. The signal component consists of $J/\psi\phi$ candidates, while background consists of $J/\psi K^+K^-$, $\psi(2S)\phi$, $\psi(2S)K^+K^-$, $\mu^+\mu^-\phi$ and $\mu^+\mu^-K^+K^-$ candidates, where $\mu^+\mu^-$ and K^+K^- indicate nonresonant contributions.

References

- [1] S. J. Brodsky and G. R. Farrar, *Scaling laws for large-momentum-transfer processes*, Phys. Rev. **D11** (1975) 1309.
- [2] C. A. Bertulani and G. Baur, *Electromagnetic processes in relativistic heavy ion collisions*, Physics Reports **163** (1988) 299.
- [3] L. A. Harland-Lang, V. A. Khoze, and M. G. Ryskin, *Exclusive production of double J/ψ mesons in hadronic collisions*, Journal of Physics G: Nuclear and Particle Physics **42** (2015) 055001.
- [4] V. P. Goncalves, B. D. Moreira, and F. S. Navarra, *Double vector meson production in photon-hadron interactions at hadronic colliders*, Eur. Phys. J. **C76** (2016) 388, arXiv:1605.05840.
- [5] X.-A. Pan *et al.*, *Photoproduction of the double J/ψ (Υ) at the LHC with forward proton tagging*, Phys. Rev. **D99** (2019) 014029.
- [6] P. Lebiedowicz, O. Nachtmann, and A. Szczurek, *Exclusive diffractive production of $\pi^+\pi^-\pi^+\pi^-$ via the intermediate $\sigma\sigma$ and $\rho\rho$ states in proton-proton collisions within tensor pomeron approach*, Phys. Rev. **D94** (2016) 034017, arXiv:1606.05126.
- [7] B. D. Moreira, C. A. Bertulani, V. P. Goncalves, and F. S. Navarra, *Production of exotic charmonium in $\gamma\gamma$ interactions at hadron colliders*, Phys. Rev. **D94** (2016) 094024, arXiv:1610.06604.
- [8] V. P. Goncalves and B. D. Moreira, *Probing the $X(4350)$ in $\gamma\gamma$ interactions at the LHC*, Eur. Phys. J. **C79** (2019) 7.
- [9] Y.-P. Xie and X. Chen, *Meson production in two-photon interaction in pp and pA ultraperipheral collisions at the LHC and FCC*, Int. J. Mod. Phys. **E27** (2018) 1850075.
- [10] N. Brambilla *et al.*, *The XYZ states: Experimental and theoretical status and perspectives*, Physics Reports **873** (2020) 1.
- [11] LHCb collaboration, R. Aaij *et al.*, *Observation of exotic $J/\psi\phi$ structures from amplitude analysis of $B^+ \rightarrow J/\psi\phi K^+$ decays*, Phys. Rev. Lett. **118** (2017) 022003, arXiv:1606.07895.
- [12] LHCb collaboration, R. Aaij *et al.*, *Amplitude analysis of $B^+ \rightarrow J/\psi\phi K^+$ decays*, Phys. Rev. **D95** (2017) 012002, arXiv:1606.07898.
- [13] LHCb collaboration, R. Aaij *et al.*, *Observation of new resonances decaying to $J/\psi K^+$ and $J/\psi\phi$* , Phys. Rev. Lett. **127** (2021) 082001, arXiv:2103.01803.
- [14] S. J. Brodsky and R. F. Lebed, *QCD dynamics of tetraquark production*, Phys. Rev. **D91** (2015) 114025.
- [15] A. Cerri *et al.*, *Opportunities in flavour physics at the HL-LHC and HE-LHC*, CERN Yellow Rep. Monogr. **7** (2019) 867, arXiv:1812.07638.

- [16] A. Esposito, C. A. Manzari, A. Pilloni, and A. D. Polosa, *Hunting for tetraquarks in ultraperipheral heavy ion collisions*, Phys. Rev. **D104** (2021) 114029.
- [17] A. Esposito, F. Piccinini, A. Pilloni, and A. D. Polosa, *A mechanism for hadron molecule production in $p\bar{p}(p)$ collisions*, Journal of Modern Physics **4** (2013) 1569.
- [18] LHCb collaboration, A. A. Alves Jr. *et al.*, *The LHCb detector at the LHC*, JINST **3** (2008) S08005.
- [19] LHCb collaboration, R. Aaij *et al.*, *LHCb detector performance*, Int. J. Mod. Phys. **A30** (2015) 1530022, [arXiv:1412.6352](#).
- [20] K. Carvalho Akiba *et al.*, *The HeRSChel detector: high-rapidity shower counters for LHCb*, JINST **13** (2018) P04017, [arXiv:1801.04281](#).
- [21] L. A. Harland-Lang, V. A. Khoze, and M. G. Ryskin, *Exclusive LHC physics with heavy ions: SuperChic 3*, The European Physical Journal **C79** (2019) 39.
- [22] N. Davidson, T. Przedzinski, and Z. Was, *PHOTOS interface in C++: Technical and physics documentation*, Comp. Phys. Comm. **199** (2016) 86, [arXiv:1011.0937](#).
- [23] Geant4 collaboration, S. Agostinelli *et al.*, *Geant4: A simulation toolkit*, Nucl. Instrum. Meth. **A506** (2003) 250.
- [24] Geant4 collaboration, J. Allison *et al.*, *Geant4 developments and applications*, IEEE Trans. Nucl. Sci. **53** (2006) 270.
- [25] M. Clemencic *et al.*, *The LHCb simulation application, Gauss: Design, evolution and experience*, J. Phys. Conf. Ser. **331** (2011) 032023.
- [26] L. A. Harland-Lang, V. A. Khoze, and M. G. Ryskin, *Exclusive physics at the LHC with SuperChic 2*, Eur. Phys. J. **C76** (2016) 9.
- [27] LHCb collaboration, R. Aaij *et al.*, *Central exclusive production of J/ψ and $\psi(2S)$ mesons in pp collisions at $\sqrt{s} = 13$ TeV*, JHEP **10** (2018) 167, [arXiv:1806.04079](#).
- [28] T. Skwarnicki, *A study of the radiative cascade transitions between the Upsilon-prime and Upsilon resonances*, PhD thesis, Institute of Nuclear Physics, Krakow, 1986, DESY-F31-86-02.
- [29] LHCb collaboration, R. Aaij *et al.*, *Precision luminosity measurements at LHCb*, JINST **9** (2014) P12005, [arXiv:1410.0149](#).
- [30] LHCb collaboration, R. Aaij *et al.*, *Measurement of the track reconstruction efficiency at LHCb*, JINST **10** (2015) P02007, [arXiv:1408.1251](#).
- [31] S. S. Wilks, *The large-sample distribution of the likelihood ratio for testing composite hypotheses*, Ann. Math. Stat. **9** (1938) 60.
- [32] LHCb collaboration, R. Aaij *et al.*, *Measurement of b -hadron branching fractions for two-body decays into charmless charged hadrons*, JHEP **10** (2012) 037, [arXiv:1206.2794](#).

D. vom Bruch¹² , V. Vorobyev⁴¹ , N. Voropaev⁴¹ , K. Vos⁷⁶ , G. Vouters¹⁰ ,
C. Vrahas⁵⁶ , J. Wagner¹⁷ , J. Walsh³² , E.J. Walton^{1,54} , G. Wan⁶ , C. Wang¹⁹ ,
G. Wang⁸ , J. Wang⁶ , J. Wang⁵ , J. Wang⁴ , J. Wang⁷¹ , M. Wang²⁷ , N. W.
Wang⁷ , R. Wang⁵² , X. Wang⁶⁹ , X. W. Wang⁵⁹ , Y. Wang⁸ , Z. Wang¹³ ,
Z. Wang⁴ , Z. Wang²⁷ , J.A. Ward^{54,1} , M. Waterlaet⁴⁶ , N.K. Watson⁵¹ ,
D. Websdale⁵⁹ , Y. Wei⁶ , B.D.C. Westhenry⁵² , D.J. White⁶⁰ , M. Whitehead⁵⁷ ,
A.R. Wiederhold⁵⁴ , D. Wiedner¹⁷ , G. Wilkinson⁶¹ , M.K. Wilkinson⁶³ ,
M. Williams⁶² , M.R.J. Williams⁵⁶ , R. Williams⁵³ , F.F. Wilson⁵⁵ , W. Wislicki³⁹ ,
M. Witek³⁸ , L. Witola¹⁹ , C.P. Wong⁶⁵ , G. Wormser¹³ , S.A. Wotton⁵³ , H. Wu⁶⁶ ,
J. Wu⁸ , Y. Wu⁶ , K. Wyllie⁴⁶ , S. Xian⁶⁹ , Z. Xiang⁵ , Y. Xie⁸ , A. Xu³² , J. Xu⁷ ,
L. Xu⁴ , L. Xu⁴ , M. Xu⁵⁴ , Z. Xu¹¹ , Z. Xu⁷ , Z. Xu⁵ , D. Yang , S. Yang⁷ ,
X. Yang⁶ , Y. Yang^{26,n} , Z. Yang⁶ , Z. Yang⁶⁴ , V. Yeroshenko¹³ , H. Yeung⁶⁰ ,
H. Yin⁸ , C. Y. Yu⁶ , J. Yu⁶⁸ , X. Yuan⁵ , E. Zaffaroni⁴⁷ , M. Zavertyaev¹⁸ ,
M. Zdybal³⁸ , M. Zeng⁴ , C. Zhang⁶ , D. Zhang⁸ , J. Zhang⁷ , L. Zhang⁴ ,
S. Zhang⁶⁸ , S. Zhang⁶ , Y. Zhang⁶ , Y. Z. Zhang⁴ , Y. Zhao¹⁹ , A. Zharkova⁴¹ ,
A. Zhelezov¹⁹ , X. Z. Zheng⁴ , Y. Zheng⁷ , T. Zhou⁶ , X. Zhou⁸ , Y. Zhou⁷ ,
V. Zhovkovska⁵⁴ , L. Z. Zhu⁷ , X. Zhu⁴ , X. Zhu⁸ , V. Zhukov¹⁶ , J. Zhuo⁴⁵ ,
Q. Zou^{5,7} , D. Zuliani^{30,q} , G. Zunica⁴⁷ .

¹*School of Physics and Astronomy, Monash University, Melbourne, Australia*

²*Centro Brasileiro de Pesquisas Físicas (CBPF), Rio de Janeiro, Brazil*

³*Universidade Federal do Rio de Janeiro (UFRJ), Rio de Janeiro, Brazil*

⁴*Center for High Energy Physics, Tsinghua University, Beijing, China*

⁵*Institute Of High Energy Physics (IHEP), Beijing, China*

⁶*School of Physics State Key Laboratory of Nuclear Physics and Technology, Peking University, Beijing, China*

⁷*University of Chinese Academy of Sciences, Beijing, China*

⁸*Institute of Particle Physics, Central China Normal University, Wuhan, Hubei, China*

⁹*Consejo Nacional de Rectores (CONARE), San Jose, Costa Rica*

¹⁰*Université Savoie Mont Blanc, CNRS, IN2P3-LAPP, Annecy, France*

¹¹*Université Clermont Auvergne, CNRS/IN2P3, LPC, Clermont-Ferrand, France*

¹²*Aix Marseille Univ, CNRS/IN2P3, CPPM, Marseille, France*

¹³*Université Paris-Saclay, CNRS/IN2P3, IJCLab, Orsay, France*

¹⁴*Laboratoire Leprince-Ringuet, CNRS/IN2P3, Ecole Polytechnique, Institut Polytechnique de Paris, Palaiseau, France*

¹⁵*LPNHE, Sorbonne Université, Paris Diderot Sorbonne Paris Cité, CNRS/IN2P3, Paris, France*

¹⁶*I. Physikalisches Institut, RWTH Aachen University, Aachen, Germany*

¹⁷*Fakultät Physik, Technische Universität Dortmund, Dortmund, Germany*

¹⁸*Max-Planck-Institut für Kernphysik (MPIK), Heidelberg, Germany*

¹⁹*Physikalisches Institut, Ruprecht-Karls-Universität Heidelberg, Heidelberg, Germany*

²⁰*School of Physics, University College Dublin, Dublin, Ireland*

²¹*INFN Sezione di Bari, Bari, Italy*

²²*INFN Sezione di Bologna, Bologna, Italy*

²³*INFN Sezione di Ferrara, Ferrara, Italy*

²⁴*INFN Sezione di Firenze, Firenze, Italy*

²⁵*INFN Laboratori Nazionali di Frascati, Frascati, Italy*

²⁶*INFN Sezione di Genova, Genova, Italy*

²⁷*INFN Sezione di Milano, Milano, Italy*

²⁸*INFN Sezione di Milano-Bicocca, Milano, Italy*

²⁹*INFN Sezione di Cagliari, Monserrato, Italy*

³⁰*INFN Sezione di Padova, Padova, Italy*

³¹*INFN Sezione di Perugia, Perugia, Italy*

³²*INFN Sezione di Pisa, Pisa, Italy*

³³*INFN Sezione di Roma La Sapienza, Roma, Italy*

- ³⁴ INFN Sezione di Roma Tor Vergata, Roma, Italy
- ³⁵ Nikhef National Institute for Subatomic Physics, Amsterdam, Netherlands
- ³⁶ Nikhef National Institute for Subatomic Physics and VU University Amsterdam, Amsterdam, Netherlands
- ³⁷ AGH - University of Krakow, Faculty of Physics and Applied Computer Science, Kraków, Poland
- ³⁸ Henryk Niewodniczanski Institute of Nuclear Physics Polish Academy of Sciences, Kraków, Poland
- ³⁹ National Center for Nuclear Research (NCBJ), Warsaw, Poland
- ⁴⁰ Horia Hulubei National Institute of Physics and Nuclear Engineering, Bucharest-Magurele, Romania
- ⁴¹ Affiliated with an institute covered by a cooperation agreement with CERN
- ⁴² DS4DS, La Salle, Universitat Ramon Llull, Barcelona, Spain
- ⁴³ ICCUB, Universitat de Barcelona, Barcelona, Spain
- ⁴⁴ Instituto Galego de Física de Altas Enerxías (IGFAE), Universidade de Santiago de Compostela, Santiago de Compostela, Spain
- ⁴⁵ Instituto de Física Corpuscular, Centro Mixto Universidad de Valencia - CSIC, Valencia, Spain
- ⁴⁶ European Organization for Nuclear Research (CERN), Geneva, Switzerland
- ⁴⁷ Institute of Physics, Ecole Polytechnique Fédérale de Lausanne (EPFL), Lausanne, Switzerland
- ⁴⁸ Physik-Institut, Universität Zürich, Zürich, Switzerland
- ⁴⁹ NSC Kharkiv Institute of Physics and Technology (NSC KIPT), Kharkiv, Ukraine
- ⁵⁰ Institute for Nuclear Research of the National Academy of Sciences (KINR), Kyiv, Ukraine
- ⁵¹ University of Birmingham, Birmingham, United Kingdom
- ⁵² H.H. Wills Physics Laboratory, University of Bristol, Bristol, United Kingdom
- ⁵³ Cavendish Laboratory, University of Cambridge, Cambridge, United Kingdom
- ⁵⁴ Department of Physics, University of Warwick, Coventry, United Kingdom
- ⁵⁵ STFC Rutherford Appleton Laboratory, Didcot, United Kingdom
- ⁵⁶ School of Physics and Astronomy, University of Edinburgh, Edinburgh, United Kingdom
- ⁵⁷ School of Physics and Astronomy, University of Glasgow, Glasgow, United Kingdom
- ⁵⁸ Oliver Lodge Laboratory, University of Liverpool, Liverpool, United Kingdom
- ⁵⁹ Imperial College London, London, United Kingdom
- ⁶⁰ Department of Physics and Astronomy, University of Manchester, Manchester, United Kingdom
- ⁶¹ Department of Physics, University of Oxford, Oxford, United Kingdom
- ⁶² Massachusetts Institute of Technology, Cambridge, MA, United States
- ⁶³ University of Cincinnati, Cincinnati, OH, United States
- ⁶⁴ University of Maryland, College Park, MD, United States
- ⁶⁵ Los Alamos National Laboratory (LANL), Los Alamos, NM, United States
- ⁶⁶ Syracuse University, Syracuse, NY, United States
- ⁶⁷ Pontifícia Universidade Católica do Rio de Janeiro (PUC-Rio), Rio de Janeiro, Brazil, associated to ³
- ⁶⁸ School of Physics and Electronics, Hunan University, Changsha City, China, associated to ⁸
- ⁶⁹ Guangdong Provincial Key Laboratory of Nuclear Science, Guangdong-Hong Kong Joint Laboratory of Quantum Matter, Institute of Quantum Matter, South China Normal University, Guangzhou, China, associated to ⁴
- ⁷⁰ Lanzhou University, Lanzhou, China, associated to ⁵
- ⁷¹ School of Physics and Technology, Wuhan University, Wuhan, China, associated to ⁴
- ⁷² Departamento de Física, Universidad Nacional de Colombia, Bogota, Colombia, associated to ¹⁵
- ⁷³ Universität Bonn - Helmholtz-Institut für Strahlen und Kernphysik, Bonn, Germany, associated to ¹⁹
- ⁷⁴ Eotvos Lorand University, Budapest, Hungary, associated to ⁴⁶
- ⁷⁵ Van Swinderen Institute, University of Groningen, Groningen, Netherlands, associated to ³⁵
- ⁷⁶ Universiteit Maastricht, Maastricht, Netherlands, associated to ³⁵
- ⁷⁷ Tadeusz Kosciuszko Cracow University of Technology, Cracow, Poland, associated to ³⁸
- ⁷⁸ Universidade da Coruña, A Coruna, Spain, associated to ⁴²
- ⁷⁹ Department of Physics and Astronomy, Uppsala University, Uppsala, Sweden, associated to ⁵⁷
- ⁸⁰ University of Michigan, Ann Arbor, MI, United States, associated to ⁶⁶
- ⁸¹ Departement de Physique Nucleaire (SPhN), Gif-Sur-Yvette, France

^a Universidade de Brasília, Brasília, Brazil

^b Centro Federal de Educação Tecnológica Celso Suckow da Fonseca, Rio De Janeiro, Brazil

^c Hangzhou Institute for Advanced Study, UCAS, Hangzhou, China

^d School of Physics and Electronics, Henan University, Kaifeng, China

- ^e *LIP6, Sorbonne Université, Paris, France*
^f *Excellence Cluster ORIGINS, Munich, Germany*
^g *Universidad Nacional Autónoma de Honduras, Tegucigalpa, Honduras*
^h *Università di Bari, Bari, Italy*
ⁱ *Università degli studi di Bergamo, Bergamo, Italy*
^j *Università di Bologna, Bologna, Italy*
^k *Università di Cagliari, Cagliari, Italy*
^l *Università di Ferrara, Ferrara, Italy*
^m *Università di Firenze, Firenze, Italy*
ⁿ *Università di Genova, Genova, Italy*
^o *Università degli Studi di Milano, Milano, Italy*
^p *Università degli Studi di Milano-Bicocca, Milano, Italy*
^q *Università di Padova, Padova, Italy*
^r *Università di Perugia, Perugia, Italy*
^s *Scuola Normale Superiore, Pisa, Italy*
^t *Università di Pisa, Pisa, Italy*
^u *Università della Basilicata, Potenza, Italy*
^v *Università di Roma Tor Vergata, Roma, Italy*
^w *Università di Siena, Siena, Italy*
^x *Università di Urbino, Urbino, Italy*
^y *Universidad de Alcalá, Alcalá de Henares, Spain*
^z *Department of Physics/Division of Particle Physics, Lund, Sweden*
[†] *Deceased*